

The iron-coating role on the oxidation kinetics of a pyritic sludge doped with fly ash

Rafael Pérez-López^{a,*}, Jordi Cama^b, José Miguel Nieto^a, Carles Ayora^b

^a *Geology Department, University of Huelva, Campus "El Carmen", E-21071 Huelva, Spain*

^b *Institute of Earth Sciences "Jaume Almera", CSIC, Lluís Solé i Sabarís s/n, E-08028 Barcelona, Spain*

Received 31 July 2006; accepted in revised form 23 January 2007; available online 30 January 2007

Abstract

The present study examines the processes that control the oxidation attenuation of a pyrite-rich sludge (72 wt% pyrite) from the Iberian Pyrite Belt by the buffer capacity of a fly ash from Los Barrios power station (S Spain), using saturated column experiments. In addition, in order to understand the behaviour of both materials inside these experiments, a fly-ash leaching test and flow-through experiments with pyritic sludge were carried out. The fly-ash leaching test showed that after leaching this material with a slightly acid solution (Millipore MQ water; pH 5.6) the pH raised up to 10.2 and that the metals released by the fly-ash dissolution did not increase significantly the metal concentrations in the output solutions. The flow-through experiments with the pyritic sludge were performed at pH 9, 22 °C and O₂ partial pressure of 0.21 atm, to calculate the dissolution rate of this residue simulating the fly-ash addition. In the experiments Fe bearing oxyhydroxides precipitated as the sludge dissolved. In two non-stirred experiments the iron precipitates formed Fe-coatings on the pyrite surfaces preventing the interaction between the oxidizing agents and the pyrite grains, halting pyrite oxidation (this process is known as pyrite microencapsulation), whereas in two stirred experiments, stirring hindered the iron precipitates to coat the pyrite grains. Thus, based on the release of S (aqueous sulphate) the steady-state pyritic sludge dissolution rate obtained was $9.0 \pm 0.2 \times 10^{-11} \text{ mol m}^{-2} \text{ s}^{-1}$.

In the saturated column experiments, the sludge dissolution was examined at acidic and basic pH at 22 °C and oxygen-saturated atmosphere. In a saturated column experiment filled with the pyritic sludge, pyrite oxidation occurred favourably at pH approx. 3.7. As the leachates of the fly ash yielded high basic pH, in another saturated column, consisting of an initial thick layer of fly-ash material and a layer of pyritic sludge, the pyrite dissolution took place at pH approx. 10.45. In this experiment, iron was depleted completely from the solution and attenuation of the sludge oxidation was produced in this conditions. The attenuation was likely promoted by precipitation of iron-bearing phases upon the pyritic surface forming Fe-coatings (of ferrihydrite and/or Fe(III) amorphous phases) that halted the pyrite oxidation (as in non-stirred flow-through experiments). Results suggest that buffering capacity of fly ash can be used to attenuate the pyrite-rich sludge oxidation.

© 2007 Elsevier Ltd. All rights reserved.

1. INTRODUCTION

The Iberian Pyritic Belt (IPB) (SW Iberian Peninsula) is one of the largest metallogenetic provinces of massive poly-metallic sulphide in the world. As a consequence, a considerable amount of mining waste dispersed in mine tailings

and mounds exist all over the region. Pyrite is the most abundant mineral in the massive sulphur deposits and in the sulphide-rich mining waste. In addition to pyrite, other minor metallic sulphides exist in mining waste (i.e., chalcopyrite CuFeS₂, galena PbS, sphalerite ZnS, arsenopyrite AsFeS) that when oxidize release metals and metalloids in solution (i.e., Cu, Pb, Zn and As). The result of sulphide oxidation processes is an extremely acid leachate containing high concentrations of sulphate, iron and other heavy metals, known as Acid Mine Drainage (AMD) (Parker and

* Corresponding author.

E-mail address: rafael.perez@dgeo.uhu.es (R. Pérez-López).

Robertson, 1999). The AMD generation as a result of the sulphide oxidative dissolution is the main pollution process of natural watercourses in the IPB (Olías et al., 2004), and in other mining environments with sulphide-rich residues.

A variety of treatments for the acid neutralization and metal retention is widely undertaken to remediate AMD contaminated sites. Several recent works report on different experimental techniques and materials to be used to remediate metal contamination. Jurjovec et al. (2002) studied the effect that carbonate minerals produces on the neutralization and metal retention processes of AMD in mine tailings by means of column experiments. In rich-sulphide mining wastes which do not contain acid neutralizing minerals, the addition of limestone is the most commonly employed treatment to the acid neutralization and metal retention transported in AMD (Nicholson et al., 1988, 1990; Mylona et al., 2000; and others). Mylona et al. (2000) showed the efficiency of limestone additive to rich-pyrite residue in inhibiting acid generation in column experiments. The presence of alkaline substances favours that pyrite (and other minor sulphides) is oxidized at high pH values, which has a double positive effect. On one hand, acidity is neutralized and concentration of Fe released during the oxidation is depleted. The Fe(III) produced by the Fe(II) oxidation, a very fast process at alkaline pH (Singer and Stumm, 1970), precipitates as ferric hydroxide, removing Fe (and other metals) from the solution. And on the other hand, the precipitation of Fe-phases on pyrite surface prevents further contact between oxidizing agents and the pyrite, and the oxidation process halts at the time. This process, described by Evangelou (1995), is known as pyrite microencapsulation.

However, some investigations challenge the effectiveness of the carbonate minerals addition to prevent the mining waste oxidation (Hood, 1991; Evangelou and Huang, 1993; Evangelou et al., 1998; and others). These authors propose that in near neutral and alkaline environments, HCO_3^- and CO_3^{2-} react with pyrite surface and form some weak Fe-carbonate complexes which accelerate non-microbial pyrite oxidation rate. Vandiviere and Evangelou (1998) and Evangelou (2001) used other alkaline reagents to study the pyrite microencapsulation process. These authors propose the addition of a solution composed of hydrogen peroxide (H_2O_2) and sodium acetate (NaOAc) to a pyritic waste. During the leaching process, H_2O_2 oxidizes pyrite and releases Fe(III) which precipitates on pyritic surface so that forming a coating on pyrite surfaces. NaOAc is used to maintain the pH of about 6. The use of potassium dihydrogen phosphate (KH_2PO_4) or silicic acid (H_4SiO_4) in the solution utilized to treat the pyrite oxidation favours that the coating composition may be ferric phosphate or ferric silicate. In both cases, this coating prevents oxidizing agents dissolving the pyritic grains and oxidation is halted. However, the use of alkaline solutions implies a high economic and environmental cost, because these reagents are “resources” and not “residues”.

The aim of this work is to prove the efficiency of the fly ash from Los Barrios power plant to attenuate the oxidation of pyrite-rich residues. Fly-ash material has been used as cement raw material, and as a partial replacement

for cement in concrete. However, the global production of fly ash exceeds their potential uses (Manz, 1997). The countries with a higher production of fly ash are China, Russia and the United States of America, although only around a 30% of the total production is utilized as a construction material. Therefore, this material is an important waste product and its potential use to treat AMD may represent a new application, in this case to neutralize another waste product.

Querol et al. (2001a) conducted a study of major and trace water soluble elements in six Spanish fly ashes by means of leaching experiments. Solutions generated by the leaching of fly ash were characterized by a very alkaline pH (upper than 10) and relatively high concentrations of Ca, Si, Al and S. At present, numerous investigations are focused on the search of new applications for this residue as an effective technique in metal retention processes in contaminated soils (Ayala et al., 1998; Brake et al., 2003; Dermatas and Meng, 2003). Other studies are focused on the use of fly ash to synthesize zeolites to be applicable as filter material in water decontamination and gas retention (Moreno et al., 2001; Querol et al., 2001b; Cama et al., 2005).

In view of the potential use of the fly ash to attenuate the acidity generated by the pyrite sludge aqueous oxidation, the main objective of the present work is to understand the processes that control the attenuation due to the fly-ash buffer capacity. Thus the pyrite oxidation in alkaline media is studied and compared to oxidation under acidic conditions by means of column experiments. The strong alkaline character of the fly ash to neutralize the acidity and to reduce the high metal content of the sludge drainages is examined by carrying out a column leaching test. Moreover, non-stirred and stirred flow-through experiments with pyritic sludge are carried out to obtain the pyrite dissolution rate at alkaline pH.

2. EXPERIMENTAL METHODOLOGY

2.1. Sample characterization

Two samples were used in the present study: (1) pyritic sludge collected from Cueva de la Mora tailings dam (IPB), and (2) fly ash as a by-product derived from the coal combustion in the Los Barrios power plant (Cádiz, S Spain).

2.1.1. Pyritic sludge

The size particle ranges from 10 to 100 μm with a median size of 25 μm , as determined by laser diffraction. X-ray diffraction (XRD) patterns show that the sludge is made up of pyrite (FeS_2 ; 72 wt%), barite (BaSO_4 ; 10 wt%), quartz (SiO_2 ; 7 wt%), K-feldspar (KAlSi_3O_8 , 6 wt%) and muscovite ($\text{KAl}_2(\text{Si}_3\text{Al})\text{O}_{10}(\text{OH}, \text{F})_2$; 4 wt%). Galena (PbS), chalcopyrite (CuFeS_2), sphalerite (ZnS) and arsenopyrite (FeAsS) are present as minor phases that were identified by means of scanning electron microscopy equipped with an energy dispersive system for microanalysis (SEM-EDS). The chemical composition analyzed with X-ray fluorescence (XRF) shows high content of S and Fe (49.8 wt%

SO₃ and 30.5 wt% Fe₂O₃) with significant amounts of potentially toxic elements such as Pb (0.8%), Zn (0.1%), As (0.1%), Cu (0.08%), Sr (0.07%) and Sb (0.02%). Based on the concentration of Pb, Cu, Zn and As, a proportion of 0.9, 0.2, 0.2 and 0.2 wt% was estimated for galena, chalcopyrite, sphalerite and arsenopyrite, respectively. The specific surface area is $1.44 \pm 0.035 \text{ m}^2 \text{ g}^{-1}$ as determined by BET gas adsorption method. SEM images of the pyritic sludge show that the grains are irregular with an angular to sub-angular shape as a consequence of grinding the raw material during the ore processing (Fig. 1a).

To get rid of secondary minerals (undetectable by XRD) that likely formed as sulphide-oxidation products such as copiapite (Fe²⁺Fe³⁺₄(SO₄)₆(OH)₂ · 20(H₂O)) and other Fe–Cu and other metals hydrated sulphates, some pyritic sludge was cleaned by flushing Millipore MQ water (18.2 MΩ) repeatedly until the supernatant was colourless. SEM images of the washed sludge reveal no changes on grains morphology compared to those of the untreated sludge, and the specific surface area of the washed sludge and those of samples retrieved after experiments are the same (within error) than the one of the raw sludge.

2.1.2. Fly ash

Size distribution analysis obtained by laser diffraction indicates that the particles have a median size of 40 μm, and spherical shape as observed by SEM (Fig. 1b). The BET-determined specific surface area is $0.63 \pm 0.022 \text{ m}^2 \text{ g}^{-1}$. XRD patterns reported by Querol et al. (2001a) showed that Los Barrios fly ash is composed of mullite (20.8 wt%), quartz (4.5%), lime (4.1%), anhydrite (1.3%), K-feldspar (2.5%), magnetite (0.5%) and glass (66.4%). The chemical composition measured by XRF shows that Los Barrios fly ash is a residue rich in Si (41.3 wt% SiO₂), Al (27.5 wt% Al₂O₃), C (16 wt% CO₂), Ca (5 wt% CaO), and Fe (3.3 wt% Fe₂O₃) with minor elements (wt%): Sr (0.3%), Cl (0.02%), Cr (0.01%), Ni (0.02%), Zn (0.01%), V (0.01%), Cu (0.01%), Co (0.01%) and Sc (0.003%). The presence of high alkali concentration contained in the most soluble phases (lime and glass phase) accounts for the high acid neutralizing potential of the fly ash.

After the experiments, the mineralogical composition of reacted materials was determined using XRD and SEM-EDS.

2.2. Experimental setup

Non-stirred and stirred flow-through experiments were used to obtain the dissolution rate of the pyrite-rich sludge at basic pH (Fig. 2a), simulating the addition of an alkaline substance (e.g., fly ash). Column experiments were conducted to lixiviate the fly ash and to study the chemical evolution of the pyritic sludge in contact with a fly-ash layer (Fig. 2b–d). Input solutions passed through all experiments (reactors and columns) with constant flow-rate of $0.050 \pm 0.005 \text{ mL min}^{-1}$ using a peristaltic pump. Output solutions were collected every 24 h after passing through a 0.45 μm Millipore Durapore filter. All the experiments were performed at 22 °C and oxygen-saturated atmosphere (atmospheric conditions).

2.2.1. Flow-through experiments

Flow-through experiments were carried out using flow-through Plexiglass reactors (ca. 40 cm³ in volume). In the non-stirred reactor cell the sample settled down at the bottom cell, whereas in the stirred experiment the sample was suspended by means of a stirred magnet bar in contact with the powder. In both reactors a 0.45 μm Millipore Durapore filter is placed at the upper part of the cell (Fig. 3). The residence time in the flow-through experiments was 13 h approximately. The flow-through experiments were conducted using both raw and cleaned pyritic sludge (Table 1). Input solutions were prepared at pH 9 with Millipore MQ water and analytical-grade sodium tetraborate decahydrate (Na₂B₄O₇ · 10 H₂O) and HCl reagents (Merck), to avoid atmospheric CO₂ interaction.

2.2.2. Column experiments

Three column experiments were carried out using Plexiglass columns: (1) a leaching test consisted of a saturated column of ca. 5 cm³ of volume (0.56 cm in diameter and 5 cm in length) filled with fly ash (ca. 7.5 g); (2) a saturated column of 2.5 cm in diameter and 18 cm in length (column I) packed with a mixture of 10 wt% pyritic sludge and 90 wt% of inert quartz to ensure permeability and (3) a saturated column of 2.5 cm in diameter and 24 cm in length (column II) packed with a lower 6 cm thick layer of fly ash and topped up with the same mixture of sludge and quartz sand (1:10). In these experiments the input solution was Millipore MQ water (18 MΩ; pH of ca. 5.6), circulating through the columns continuously from bottom upwards.

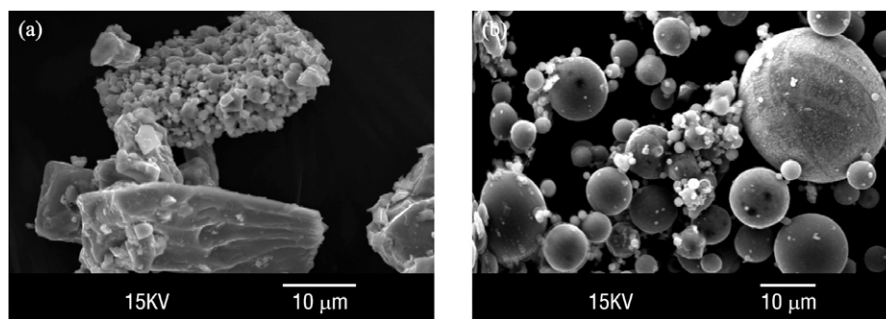


Fig. 1. SEM images of (a) pyritic sludge and (b) fly ash.

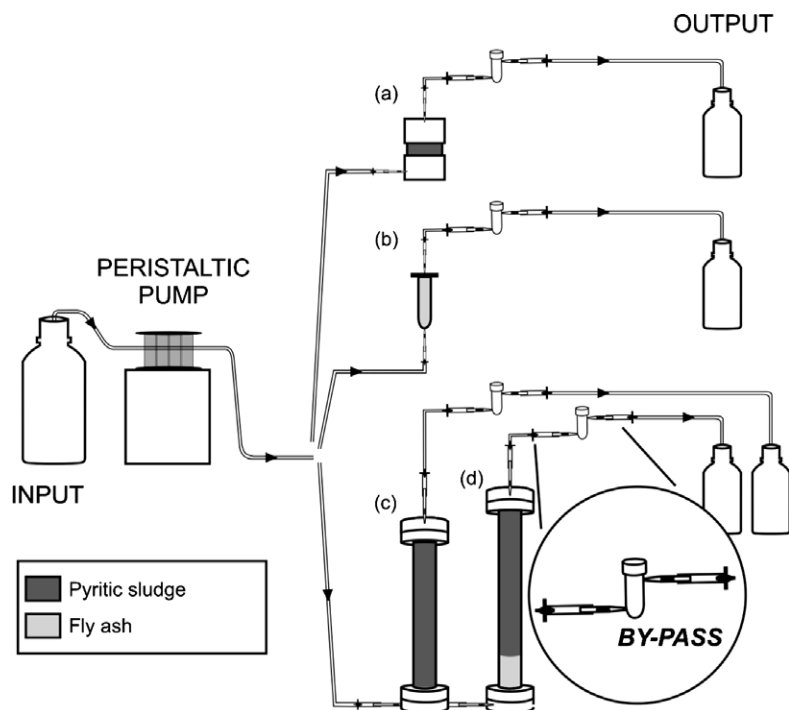


Fig. 2. Scheme showing the experimental design and the different types of experiments carried out: (a) flow-through experiments, (b) fly-ash leaching test, (c) saturated column I (18 cm in length) and (d) saturated column II (24 cm in length). pH of input solutions was 9 in the flow-through experiments and ca. 5.6 in the column experiments.

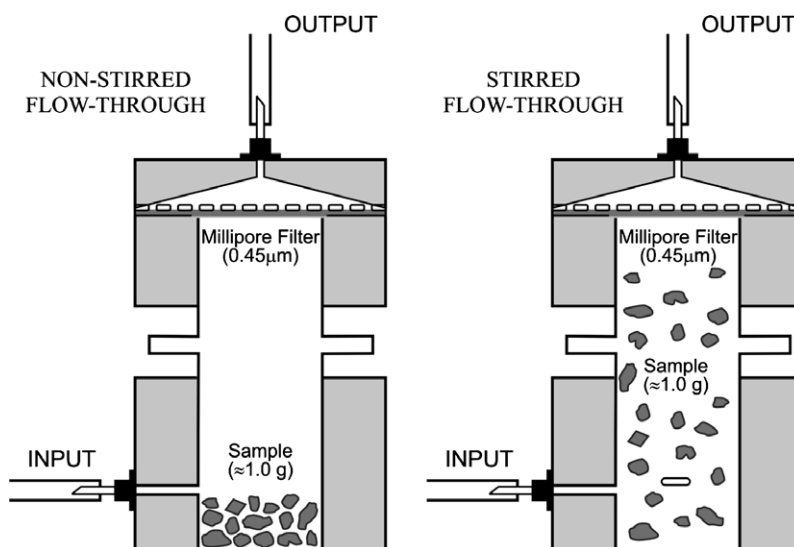


Fig. 3. Experimental design of the reaction cells used in the non-stirred and stirred flow-through experiments.

The residence times in the experiments were approximately 1.6, 118 and 157 h in the leaching test, column I and column II, respectively. Output solutions were collected every 24 h after passing through a 0.45 μm Millipore Durapore filter.

2.3. Solutions

All input solutions were equilibrated with a constant O_2 partial pressure of 0.21 ± 0.01 atm by means of Alphagaz

bottles for 12 h. Total concentrations of Al, As, Ba, Ca, Cu, Fe, K, Mg, Na, Pb, S, Si and Zn of input and output solutions were analysed with ICP-AES. The analytical error in the concentrations was 4%. The detection limit for Fe and S was determined to be 0.1, and 0.5 μM for the other elements. Input and output solution pH was measured with a Crison[®] combined glass electrode at room temperature (22 ± 2 °C) using a by-pass cell to avoid CO_2 interaction with the atmosphere. The pH error is 0.02 pH units.

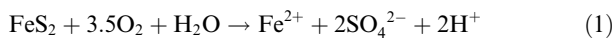
Table 1
Experimental conditions and results of the flow-through experiments

Experiment	Initial mass (g)	Sample	Flow rate (mL min ⁻¹)	Reactor	Experimental duration (h)	pH output	S output (μM)	R (mol m ⁻² s ⁻¹)	Error R (%)
LDP-25-1	1.008	Raw	0.048	Non-stirred	356	8.87	DL	—	—
LDP-25-2	1.008	Raw	0.050	Stirred	552	8.84	195.86	8.9E-11	15
LDP-25-3	1.002	Washed	0.053	Non-stirred	951	8.86	DL	—	—
LDP-25-4	1.008	Washed	0.044	Stirred	551	8.85	244.91	9.2E-11	15

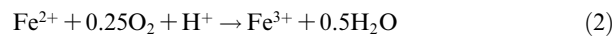
DL means concentrations below of the detection limit of the ICP-AES.

3. DISSOLUTION RATE AND EXPERIMENTAL ERROR

The overall dissolution reaction of the pyrite in the pyritic sludge (72 wt%), under the conditions studied, can be expressed as (Singer and Stumm, 1970):



The Fe(II) released is oxidized to Fe(III) according to Eq. (2), and the Fe(III) is hydrolyzed to form ferric hydroxide at pH greater than 3.5 (Eq. (3)).



In a flow-through experiment, the steady-state dissolution rate of a mineral (mol m⁻² s⁻¹), R , can be calculated according to the mass balance equation:

$$v_i R = \frac{q}{A_{\min}} (C_{i,\text{output}} - C_{i,\text{input}}) \quad (4)$$

where v_i is the stoichiometry coefficient of the component i in the dissolution reaction, A_{\min} is the reactive surface area (m²) of the mineral, q is the fluid volume flux through the system (m³ s⁻¹) and $C_{i,\text{input}}$ and $C_{i,\text{output}}$ are the concentrations of component i in the input and output solutions (mol m⁻³), respectively.

The pyritic sludge is constituted by a set of minerals; nevertheless, its dissolution is controlled exclusively by pyrite dissolution (Domènech et al., 2002). Hence, in the flow-through experiments, using the release of total S (aqueous sulphate) at steady state and based on Eq. (4) allows to accurately compute the pyrite dissolution rate, since the amount of S released by the rest of minor sulphides is practically negligible. The total surface area of pyrite (A_{pyrite}) is:

$$A_{\text{pyrite}} = A_{\text{BET}} m_{\text{sludge}} \%_{\text{pyrite}} \quad (5)$$

where A_{BET} is the BET surface area (m² g⁻¹), m_{sludge} is the mass of sludge used in the experiments (g) and $\%_{\text{pyrite}}$ is the percentage of pyrite in the sludge ($g_{\text{pyrite}} g_{\text{sludge}}^{-1}$).

The error in the calculated dissolution rate (ΔR) is estimated by means of the Gaussian error propagation method (Barrante, 1974), according to the equation:

$$\Delta R = \left(\left(\frac{C_{j,\text{out}}}{A_{\min} v_j} \right)^2 \cdot \Delta q^2 + \left(\frac{q \cdot C_{j,\text{out}}}{A_{\min}^2 v_j} \right)^2 \cdot \Delta A_{\min}^2 + \left(\frac{q}{A_{\min} v_j} \right)^2 \cdot \Delta C_{j,\text{out}}^2 \right)^{0.5} \quad (6)$$

Steady-state dissolution rates were calculated using the specific surface area value of 1.44 m² g⁻¹. The error in the cal-

culated rates was approximately 15% due to the uncertainty of the BET surface area measurement ($\pm 14.9\%$).

Solution saturation indexes with respect to solid phases (SI = log(IAP/ K_S), where SI is the saturation index, IAP is the ion activity product and K_S is the solid solubility product), and aqueous speciation of the leachates were calculated using the equilibrium geochemical speciation/mass transfer code PHREEQC (Parkhurst, 1995) and the database of the speciation code MINTeq.

4. RESULTS

4.1. Fly-ash leaching test

The leachates generated in the fly-ash leaching test yielded a pH of 10.2 ± 0.26 and relatively high concentrations of Ca, Si, Mg, Al and S ($C_{\text{Ca}} \gg C_{\text{Si}} > C_{\text{Al}} \approx C_{\text{Mg}} \approx C_{\text{S}}$) compared to the rest of elements analysed (Fig. 4). In the onset of the experiment the output pH reached a value of 12.3, most probably due to lime dissolution, and then dropped rapidly to 10.2. Based on the variation in the output concentrations as a function with time, the experimental run can be divided in three stages (Fig. 4b). In the first 100 h all the output concentrations reached a maximum except Mg_{out} that was almost totally depleted (stage A). This high release was likely due to fast dissolution of glass, quartz, anhydrite, and lime caused by the high pH and to the high reactivity of very soluble fly-ash microparticles (Fig. 1b). A second stage (B) is characterized by a gradual decrease of output concentrations with time (100–400 h) due to exhaustion of microparticles, anhydrite, and glass dissolution (Si–Al–Ca–S bearing phase). Thereafter, at stage C (400–800 h), the output concentrations reached steady-state in which Ca concentration predominated over those of Si, Mg, Al and S (310, 120, 60, 35 and 25 μM, respectively) and pH was about 10.2. The Ca source was from the glass dissolution. Release of Al, Mg, Si, and S is also from glass dissolution, together with quartz and mullite dissolution.

Calculations with PHREEQC show that the leachates are supersaturated with respect to bayerite (Al(OH)₃) through the entire experiment (thermodynamic data from Verdes et al., 1992), and supersaturated with respect to brucite (Mg(OH)₂) after 350 h (Fig. 4c). Likewise, the output solutions are supersaturated with respect to some silicates (e.g., nontronite, kaolinite and montmorillonite). Nonetheless, the experimental conditions do not favour silicate precipitation, and hence only Al and Mg concentrations could be controlled by precipitation of bayerite and brucite

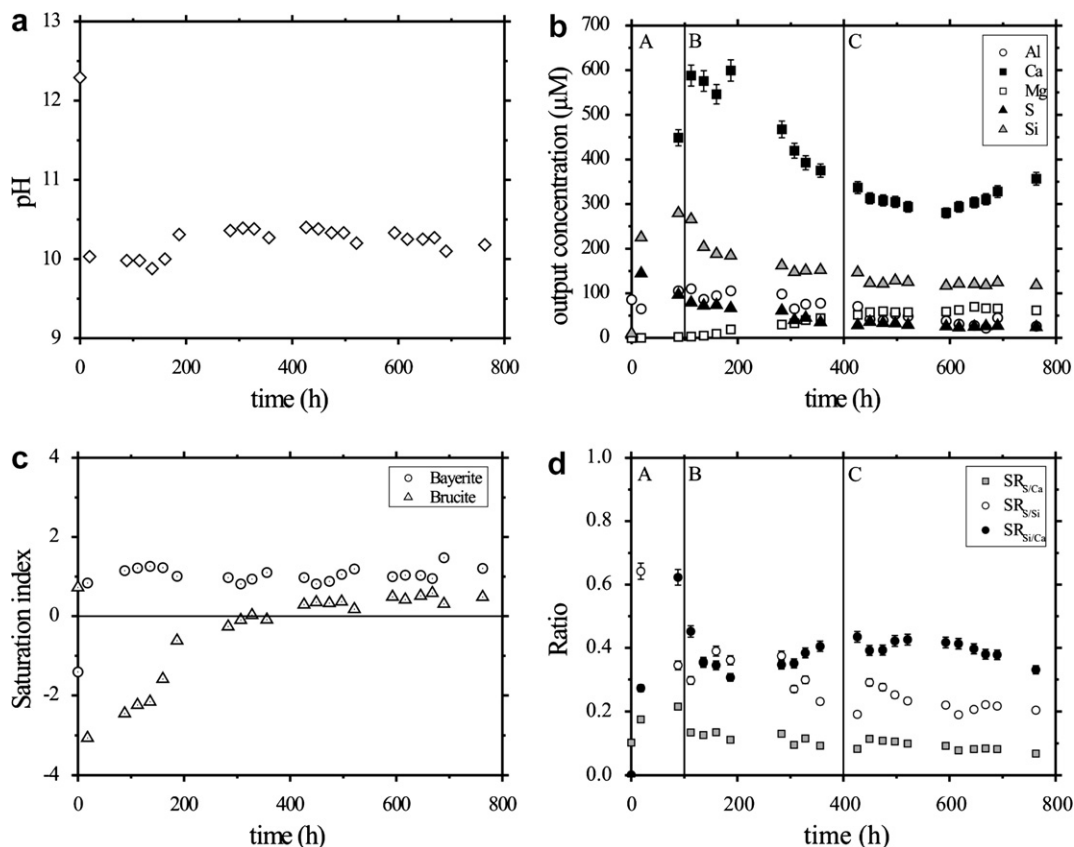


Fig. 4. Temporal variation in (a) pH, (b) output concentrations of Al, Ca, Mg, S and Si, (c) the saturation index of bayerite and brucite and (d) the stoichiometric ratios S/Ca, S/Si and Si/Ca of the leachates in the fly-ash leaching test.

respectively, as suggested by the results of the geochemical modelling. Note that a likely little amount of such precipitates is very difficult to identify by SEM images.

Based on the release of Ca, Si and S as fly ash dissolves, one can estimate the stoichiometric ratios S/Ca, S/Si and Si/Ca (Fig. 4d) that at steady state (stage C) are 0.09, 0.22 and 0.4, respectively.

4.2. Flow-through experiments

The variation of output S concentration as a function of time in the flow-through experiments at pH 8.9 with pyritic sludge is shown in Fig. 5. The experimental conditions and steady-state values of pH, output sulphur concentrations and dissolution rate are detailed in Table 1. Achievement of steady state was verified by a series of constant sulphur concentration that differed less than 5%.

4.2.1. Flow-through experiments with raw sludge

In the flow-through experiments with raw pyritic sludge, the concentrations of S, Fe and minor metals are higher at the onset of the experiment than in the rest of the experiment. These high concentrations are probably produced by the fast dissolution of secondary minerals formed during the pyritic sludge oxidation in the tailings dam. In the non-stirred flow-through experiment steady-state sulphur concentrations are below detection limit, whereas in the stirred

experiment the steady-state sulphur concentration is 196 μM (Fig. 5a). Hence, in the non-stirred experiment the pyritic sludge dissolution is practically nil and in the stirred one the steady-state dissolution rate based on sulphur release and Eq. (4) is $8.9 \times 10^{-11} \text{ mol m}^{-2} \text{ s}^{-1}$ (Table 1). In both experiments, the output Fe concentrations are below detection limit of the ICP-AES (0.1 μM) except in the first leachates. In the PHREEQC calculations, Fe is introduced with the low concentration of the ICP-AES detection limit (0.1 μM of Fe), assuming that total Fe is Fe(III) for the fast oxidation of Fe(II)–Fe(III) in highly alkaline pH (Singer and Stumm, 1970).

According to the PHREEQC modelling results, solutions are supersaturated with respect to ferrihydrite. Applying the law of mass action (Eq. (7)) and assuming that $a_{\text{H}_2\text{O}}$ equals 1 and $\log K_{\text{eq}}$ equals -4.89 , a dependence of the Fe^{3+} activity with pH (Eq. (8)) is obtained:



$$\log(a_{\text{Fe}^{3+}}) = 4.891 - 3 \cdot \text{pH} \quad (8)$$

In Fig. 5b the plot of log iron activity vs. pH based on Eq. (7) depicts ferrihydrite equilibrium (solid line) with respect to $\log(a_{\text{Fe}^{3+}})$ and pH (supersaturation and undersaturation above equilibrium and below equilibrium, respectively). It is observed that the leachates are supersaturated with respect to ferrihydrite, indicating that ferrihydrite precipita-

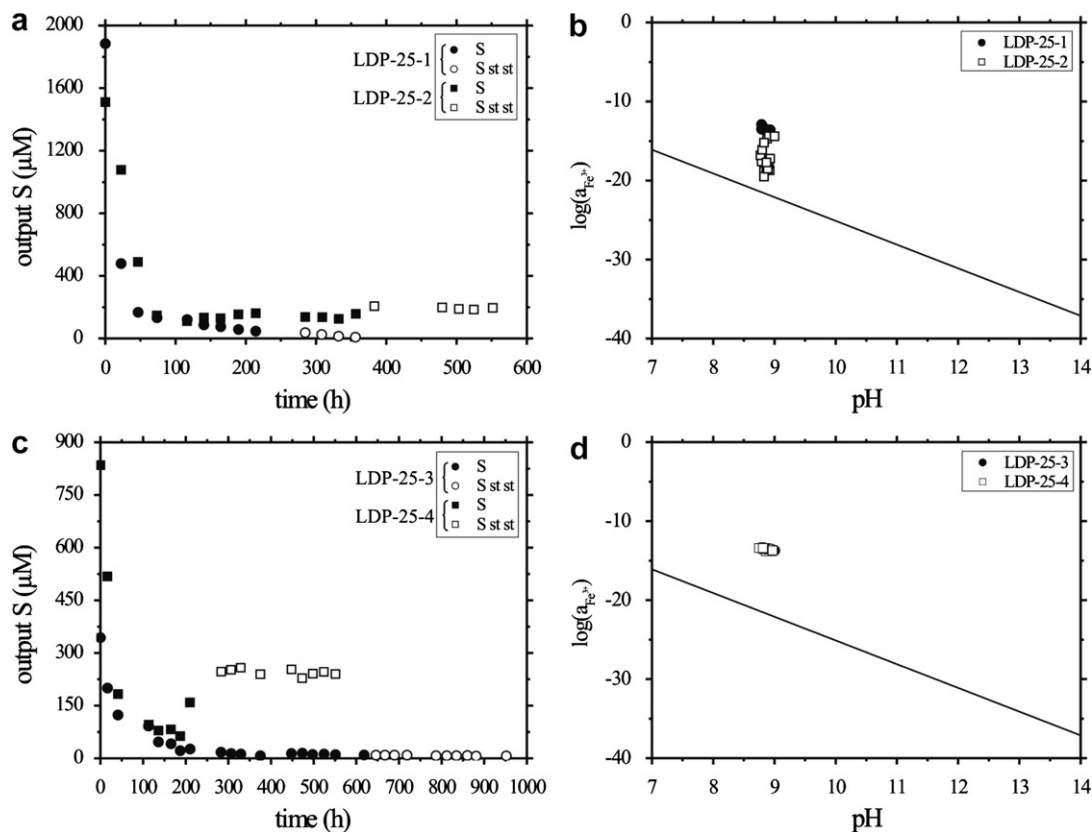


Fig. 5. Temporal variation in the output S concentration in the flow-through experiments at pH 9 with (a) raw pyritic sludge and (c) pre-cleaned pyritic sludge. Representation of $\log(a_{\text{Fe}^{+3}})$ vs. pH (line represents the equilibrium with ferrihydrite) in the flow-through experiments at pH 9 with (b) raw pyritic sludge and (d) pre-cleaned pyritic sludge. In (a) and (c), the open symbols indicates S values used to calculate average steady state.

tion would account for the aqueous iron depletion. Concentrations of Cu, Pb, Zn and As in the leachates are detected at the onset of the experiment and subsequently decrease below detection limit. This metal depletion could be attributed to metal co-precipitation as ferrihydrite is being formed (Webster et al., 1994), since precipitation of these metal-hydroxides is unlikely at this pH.

4.2.2. Flow-through experiments with washed sludge

In the flow-through experiments using washed sludge the temporal variation in concentrations of the output S, Fe and the other metals is similar to that of the raw sludge experiments with the exception of the initial leachates that are less concentrated. This is due to the fact that highly soluble secondary minerals and very reactive microparticles were removed previously by washing the sludge. In the non-stirred flow-through experiment, the steady-state output S concentration is below detection limit (ICP-AES), and thus the sludge dissolution rate is practically nil. In the stirred experiment, the steady-state sulphur concentration is 245 μM (Fig. 5c) and the steady-state pyrite dissolution rate is $9.2 \times 10^{-11} \text{ mol m}^{-2} \text{ s}^{-1}$ that is the same rate within error than the rate obtained for the raw sludge. Based on the equilibrium reaction of ferrihydrite dissolution Eq. (7) and the law of mass action Eq. (8) a plot of iron activity with respect to pH shows supersaturation of the solutions with respect to ferrihydrite in the experiments

with washed sludge (Fig. 5d). Ferrihydrite precipitation and metal co-precipitation accounts for the depletion of iron and the other metals (Cu, Pb, Zn and As), which only are detected in the leachates at the beginning of both experiments.

4.3. Saturated column experiments

4.3.1. Column I: sludge dissolution

The variation in output pH and output concentrations of S, Fe and other metals as a function of time is shown in Fig. 6. The pH of the leachate at the beginning of the experiment is very low (1.75) and the output concentrations of S, Fe, Cu, Zn and As are as high as 100, 60, 1.6, 0.8 and 0.2 mM, respectively. This high concentrations and very acid pH are caused by fast dissolution of secondary minerals making up the sludge at the beginning of the experiment (Fig. 6a,b). As the secondary minerals were completely dissolved, the pH increases and the output concentrations of S and Fe decrease until steady state is reached after 100 h. At steady-state pH and output concentrations of S and Fe are 3.70 and 140 and 38 μM , respectively (Fig. 6a,b). The oxidation of minor sulphides (e.g., chalcopyrite (CuFeS_2), sphalerite (ZnS) and arsenopyrite (AsFeS)) produced low release of Cu, Zn and As in solution such that C_{Cu} and C_{As} are 0.32 and 0.44 μM , respectively, and Zn concentration is below detection limit after 165 h (Fig. 6c).

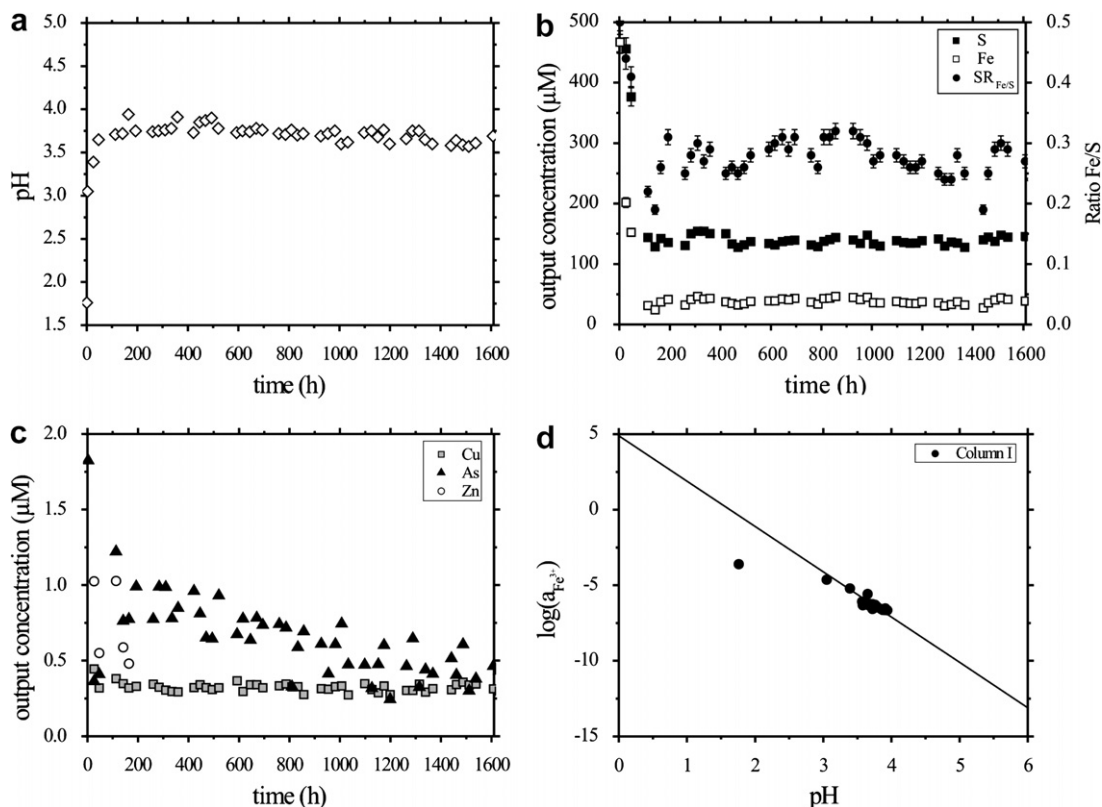


Fig. 6. Variation in (a) the pH, (b) output concentration of S and Fe (and Fe/S ratio), (c) output concentration of Cu, As and Zn in column I with time. (d) $\log(a_{\text{Fe}^{3+}})$ vs. pH (line represents the equilibrium with ferrihydrite) in column I. The initial, high concentrations are omitted to improve the figure.

PHREEQC calculations show that the leachates are in equilibrium with respect to ferrihydrite (Fig. 6d). Therefore, during oxidation, some of the Fe(II) released is oxidized to Fe(III) and precipitates as ferrihydrite until the leachates reach equilibrium with respect to it, yielding a Fe/S ratio of about 0.3, instead of 0.5 as expected from pyrite stoichiometry (Fig. 6b). The remaining aqueous iron is being transported through the column.

4.3.2. Column II: fly-ash and sludge dissolution

It was observed that pH of the first leachate is 2 and that the output concentrations are high (e.g., [S], [Fe], [Cu], [Zn] and [As] are 65, 30, 1, 0.35 and 0.1 mM, respectively) likely due to fast dissolution of secondary minerals. In the subsequent leachates, output pH abruptly increased ($10 < \text{pH} < 12$) and the output concentrations decreased, yielding instead high concentrations of Ca, Si, Al and Mg (Fig. 7a–d) as it was observed in the leachates of the fly-ash experiment.

As steady state was attained after 1100 h, it was observed that $C_{\text{Ca}} > C_{\text{S}} > C_{\text{Si}} > C_{\text{Al}} > C_{\text{Mg}}$. Leaching the fly-ash layer with a mildly acidic water (Millipore MQ water) must produce an alkaline solution that enters the sludge bed. At the beginning of the experiment, Ca concentrations of the leachates are high due to fast dissolution of the soluble phases present in the fly ash (anhydrite, lime) and the high reactivity of the corresponding microparticles. As these phases dissolve, Ca concentration decreases until stea-

dy state is reached. At this stage glass dissolution is taking place and is the main source of aqueous Ca, Si, Al and Mg whose concentrations are 470, 100, 90 and 10 μM, respectively. Aqueous sulphur is released due to pyrite oxidation and fly-ash leaching (anhydrite and glass). Based on the S release, three stages can be distinguished during the experiment (Fig. 7c). During the first 200 h (stage A), high output S concentration corresponds to fast dissolution of secondary minerals (sludge) and soluble anhydrite (fly ash), as well as the contribution of very reactive microparticles. From 200 to 1100 h (stage B) the gradual decrease of S concentration occurs as anhydrite and microparticles are being consumed, glass dissolves and pyrite oxidizes. Finally, at the third stage (C), the lowest concentrations of S are reached at steady state (113 μM) and the sulphur source is from glass dissolution and the pyrite oxidation. Aqueous iron is only detected at the first leachate (pH 2). Thereafter, the output Fe concentrations are below detection limit (0.1 μM) (Fig. 7c). Concentrations of Cu, Zn and As due to the oxidation of chalcopyrite (CuFeS_2), sphalerite (ZnS) and arsenopyrite (AsFeS), respectively, are relatively lower than the concentrations of these metals in the leachates from column I (Fig. 7d) and even below the detection limit in some leachates (e.g., steady-state concentrations of Cu and As are 0.05 and 0.18 μM, respectively, and Zn concentrations are below detection limit after 230 h). Introducing again Fe(III) (0.1 μM) in the modelling, PHREEQC calculations show that all leachates but the first one are

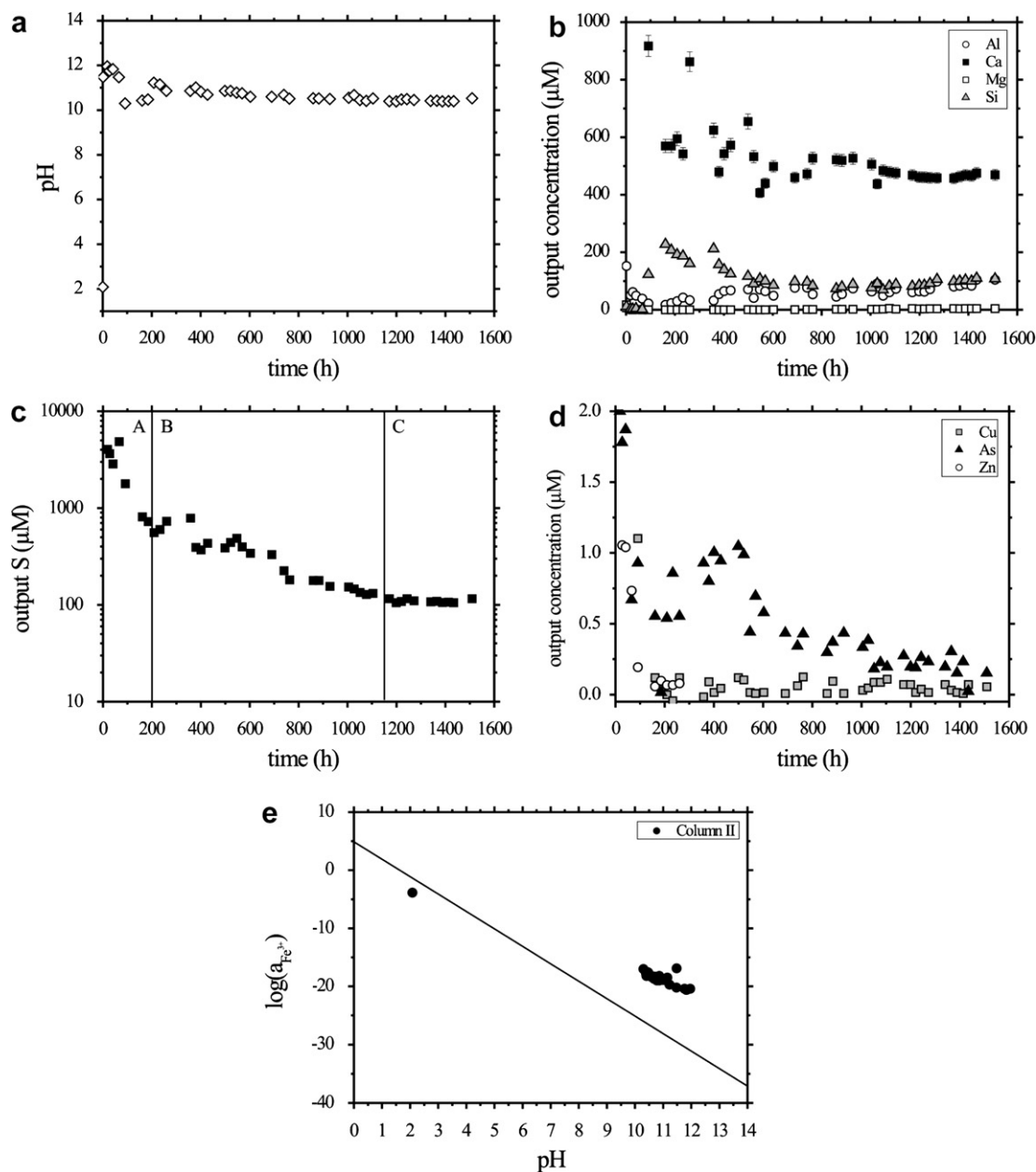


Fig. 7. Temporal variation in (a) pH, (b) output concentration of Al, Ca, Mg and Si, (c) output concentration of S, (d) output concentration of Cu, As and Zn in column II. (e) Representation of $\log(a_{\text{Fe}^{+3}})$ vs. pH (line represents the equilibrium with ferrihydrite) in column II. The initial, high concentrations are not represented to improve the figure.

supersaturated with respect to ferrihydrite (Fig. 7e). At this high pH the precipitation of ferrihydrite accounts for the absence of aqueous iron. The low concentrations of Cu and As may be explained by co-precipitation with ferrihydrite. Moreover, the leachates are highly supersaturated with respect to amorphous Al hydroxide ($\text{Al}(\text{OH})_3$).

5. DISCUSSION

5.1. Fly-ash dissolution in the leaching test

The main advantage of fly-ash addition in our experiments is that its dissolution increased the pH to 10.2. The

only possible disadvantage of fly-ash utilization is the release of some toxic elements in solution during the leaching (Querol et al., 2001a,b). However, these elements are released in much lower concentrations than in acid mine drainage. Moreover, the alkaline pH also favours the depletion of these metals due to the precipitation and/or co-precipitation/adsorption of metals oxyhydroxides. Overall, the dissolution of the fly-ash material suggests that its capacity to neutralize the sludge acidity is guaranteed by the resulting high pH, and that the low release of other metals does not contribute to increase the contamination with additional metal concentrations to the waters contaminated by acid mine drainage.

5.2. Pyritic sludge dissolution at alkaline pH in the flow-through experiments

As stated before, pyrite dissolution rate in the non-stirred flow-through experiments using raw or washed pyritic sludge was practically zero at pH 9. The explanation is that at this pH iron released by pyrite oxidation precipitates as Fe oxyhydroxides (most probably ferrihydrite) on the pyritic grains (Fig. 8). With time, Fe-precipitates coat the pyrite surfaces and prevent any interaction between the grains and aqueous oxygen. Hence, pyrite oxidation is halted (Fig. 9a). This mechanism is known as microencapsulation and was described by Evangelou (1995). However, in the stirred experiments at the same pH, aqueous sulphur was detected, and hence it was possible to calculate the pyrite dissolution rate based on aqueous sulphur. It was observed that in the stirred experiments Fe oxyhydroxides precipitation took place as suspended particles, but not over the pyrite grains (Fig. 9b). Stirring thus prevented the formation of Fe-coating upon the grains, and the pyrite oxidation continued. At this point it is possible to state that the presence of secondary minerals only affects the initial stage of pyrite dissolution, and that the effective pyrite dissolution at pH 9 depends on whether the Fe-precipitates coat the pyritic grains, i.e., under non-stirring conditions the oxidation process is halted, whereas at stirring conditions pyrite dissolution is favored.

Pyrite dissolution kinetics has been a focus of previous numerous investigations (Smith and Shumate, 1970; McKibben, 1984; Nicholson et al., 1988; Moses and Herman, 1991; and others). In particular, Williamson and Rimstidt (1994) proposed an empirical rate law of pyrite dissolution that is expressed as

$$r(\text{mol m}^{-2} \text{ s}^{-1}) = 10^{-8.19(\pm 0.1)} [\text{O}_2(\text{aq})]^{0.5(\pm 0.04)} [\text{H}^+]^{-0.11(\pm 0.01)} \quad (9)$$

This rate law is valid for a wide range of dissolved oxygen concentration and from pH 2 to 10. It is readily inferred that pyrite oxidative dissolution is affected in different degree by two environmental variables, the presence of dissolved oxygen and in a lesser extent by pH. Accordingly, an increase in dissolved oxygen increases pyrite oxidation and a decrease of pH decreases pyrite dissolution (e.g., the rate is faster at basic pH than at acid pH). This dependency of the pyrite dissolution rate with the pH and dis-

solved oxygen concentration was also shown by Holmes and Crundwell (2000). In contrast, using the dissolution rate of the pyritic sludge utilized by Domènech et al. (2002) reported in Cama and Acero (2005) at pH 3 and 250 μM DO ($1.0 \pm 0.4 \times 10^{-10} \text{ mol m}^{-2} \text{ s}^{-1}$) and the pyrite dissolution rate obtained in the present study at pH 8.9 ($9.0 \pm 0.2 \times 10^{-11} \text{ mol m}^{-2} \text{ s}^{-1}$), one can propose a non-existing pH-rate dependency. One could argue that some Fe oxyhydroxide microparticles precipitated over the pyritic grains, albeit not observed by SEM, attenuating the rate by surface passivation. Nonetheless, this seems unlikely since the amount of iron precipitated is less than 6% of the iron that should be released. Therefore, a comparison between the pyrite rate in the present study and the pyrite rate obtained by Williamson and Rimstidt (1994) at pH 8.9, calculated using Eq. (9) ($9.7 \times 10^{-10} \text{ mol m}^{-2} \text{ s}^{-1}$), yields that the dissolution rate in the present study is lower by a factor of 11. It is important to note the different specific surface area used to normalize the rates in each study. Although this difference does not eliminate the discrepancy regarding the pH-rate dependency, could explain the relative, distinct rates values.

5.3. Pyritic sludge dissolution in the saturated column experiments

5.3.1. Column I

In the columns, pyrite oxidation is taking place under saturated conditions and atmospheric oxygen partial pressure (e.g., 250 μM DO). In column I an output pH of 3.7 demonstrates that pyrite dissolution acidifies the solution passing through the column as expected (see Eq. (1)). Under these conditions and in accordance with the pyrite oxidative dissolution reaction (Eq. (1)) and the corresponding Keq ($\log \text{Keq} = 205.11$), pyrite aqueous oxidation is taking place at highly undersaturated conditions with respect to pyrite. According to the stoichiometry of this reaction if aqueous oxygen is consumed totally, the maximum concentration of S and Fe than can be released during pyrite oxidation is 143 and 71.4 μM , respectively. Therefore, according to the sulphur concentrations and pH, pyrite dissolved in the saturated porous medium until DO was totally consumed.

The Fe concentration in the leachates was lower than stoichiometrically expected, owing to aqueous sulphur concentration, and this iron deficit was likely due to fer-

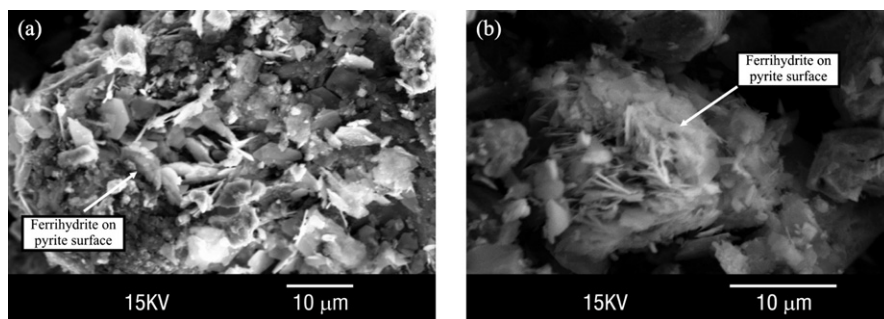


Fig. 8. SEM images of Fe oxyhydroxides coating pyritic grains in (a) the LDP-25-1 experiment and (b) the LDP-25-3 experiment.

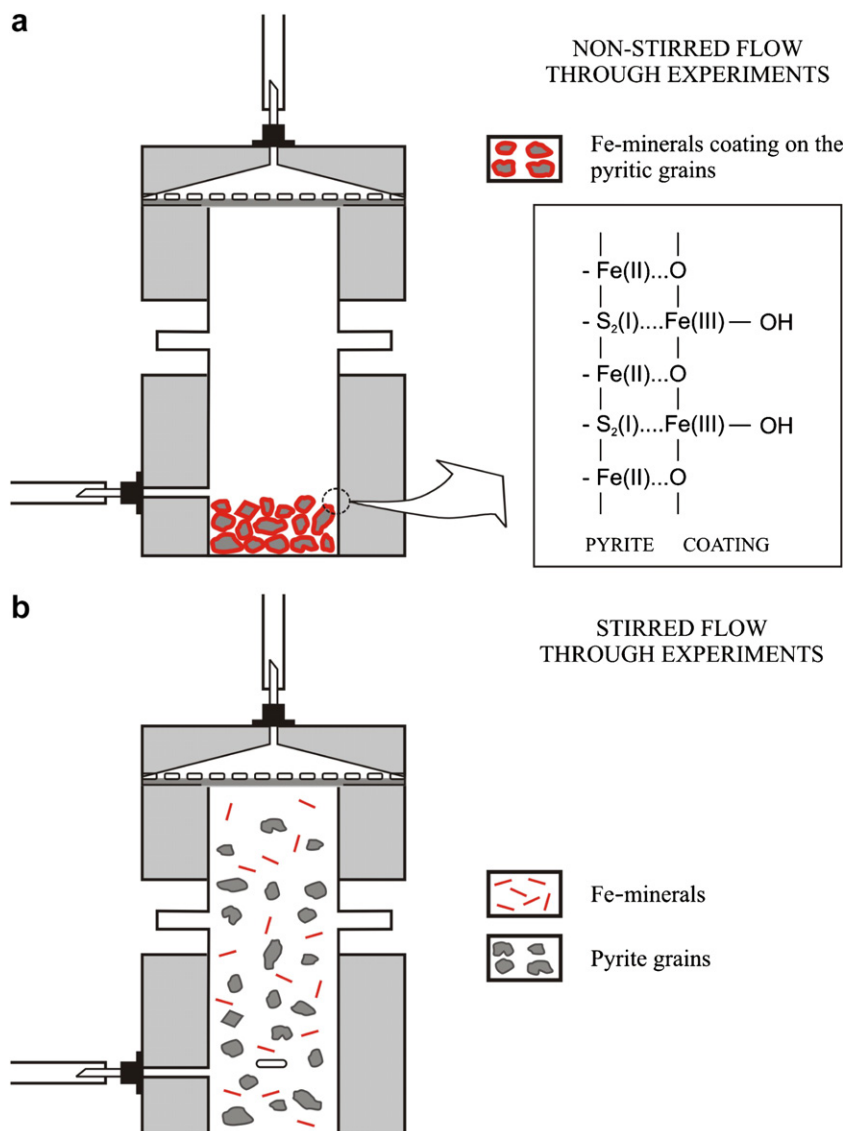


Fig. 9. Sketch drawn that shows (a) the mechanism of pyrite microencapsulation by Fe oxyhydroxide coating in the non-stirred flow through experiments, and (b) the absence of iron coating on pyrite grains in the stirred experiments. In this case Fe is precipitating as oxyhydroxides suspended particles.

rihydrite precipitation. The ferrihydrite precipitation is produced after the oxidation of Fe(II)–Fe(III) by DO (Eq. (2)). However, the amount of DO consumed by this reaction is lower than the amount consumed by the pyrite oxidation (1 mole of pyrite is oxidized by 3.5 mol of DO and produces 1 mol of Fe(II), which is oxidized to 1 mol of Fe(III) consuming only 0.25 mol of DO). The amount of DO consumed during the Fe(II) oxidation in column I probably explains that the S concentrations obtained in the leachates (140 μM), although very similar, are slightly lower than the concentrations that should be obtained according to the stoichiometry of the pyrite oxidation (143 μM). After dismantling the column, Fe-coatings over pyritic grains were not observed along the column, probably due to the low amount of Fe precipitated.

5.3.2. Column II

Unlike column I, pyrite oxidative dissolution in column II is taking place at alkaline pH (10.45) after the input solution went through the fly-ash layer and dissolved it. Assuming that pyrite oxidation should be faster at alkaline pH than at acid pH according to Eq. (9), pyrite oxidation should be faster in column II than it is in column I. Based on the DO concentration (250 μM), the maximum concentration of S and Fe releasable by pyrite oxidation cannot be higher than 143 and 71.4 μM , respectively. Nevertheless, it is important to highlight that all aqueous iron is depleted by ferrihydrite precipitation at pH 10.45. This process (see Eqs. (2) and (3)) implies the consumption of approx. 17 of 250 μM of DO. The available amount of DO to oxidize the pyrite would be approx. 233 μM , which would suppose a maximum S production of 135 μM .

The steady-state leachates had a sulphur concentration of about $113 \mu\text{M}$, representing ca. 80% of the maximum sulphur concentration expected for a total DO consumption. Nonetheless, in column II it must be considered that S was released by both the pyrite oxidation and the fly-ash leaching. At steady state, the amount of S released by fly-ash leaching can be estimated from the release of Ca and Si, based on the stoichiometric ratios (S/Ca, S/Si and Si/Ca) established in the fly-ash leaching test. Accordingly, 35% of total aqueous sulphur is released by fly-ash leaching ($40 \mu\text{M}$) and the rest by pyrite oxidation ($70 \mu\text{M}$). The mixture of sludge and sand was the same in both columns, and therefore the DO consumption should be equal, but faster in column II than in column I, since pyrite oxidation is faster at alkaline pH. This implies that S concentration of the leachates would be the sum of the maximum concentration released in the oxidation process ($135 \mu\text{M}$), plus the concentration resulting from the fly-ash leaching ($40 \mu\text{M}$), yielding a total S concentration of $175 \mu\text{M}$. However, the lower steady-state sulphur concentration obtained ($113 \mu\text{M}$) must be the sum of S following the fly-ash dissolution ($40 \mu\text{M}$) and the 50% of the maximum S concentration released in the sludge oxidation (ca. $70 \mu\text{M}$). Since the leachates are undersaturated with respect to any S-phase (e.g., jarosite or schwertmannite), and no other phase precipitates along the column that might retain part of the S released in solution, a feasible explanation accounting for the sulphur deficit is that pyrite oxidation is attenuated at high pH.

The proposed attenuation mechanism is that the iron precipitates as Fe oxyhydroxides together with other metals (co-precipitation) over the pyritic grains forming coatings. These Fe-bearing phases (Fig. 10) (similar to the ones observed in the non-stirred flow-through experiment at pH 9) that rapidly grow in thickness, would obstruct DO to

reach the surfaces and thus halt pyrite dissolution. This results in an overall attenuation of the pyrite oxidation process, that is to say a process of microencapsulation. Due to the small size of the newly formed phases covering the pyrite grains, a quantification of their chemical composition was impossible. Fig. 10d shows the EDS pattern of a raw pyrite grain before the experiment (P1; Fig. 10a) and a pyrite grain with the coating from the column II, collected after the experiment (P2, P3, P4; Fig. 10b,c). The EDS patterns of P2, P3 and P4 show a progressive Fe enrichment with respect to the EDS pattern of P1. In addition, when the electron beam from SEM hit in a progressively oblique way on the coated pyrite surface, it was observed an increase in Fe with respect to S in the EDS patterns, given that the excitation zone is much more superficial and it does not penetrate in the pyrite grain. Therefore, the phases covering the pyrite grains are Fe-bearing phases, likely ferrihydrite as suggested by chemical equilibrium calculations.

In a column, encapsulation of pyrite grains would progress in the flux direction (from the bottom to the top in column II). The reason that pyrite was still oxidizing was the existence of a non-coated pyrite fraction. After 1500 h microencapsulation was partially affecting the pyritic sludge as indicates an output sulphur concentration of $113 \mu\text{M}$ ($70 \mu\text{M}$ from pyrite oxidation), since the remaining sludge was still oxidizing. At the end of the experiment, ochre precipitates, indicating the presence of Fe-bearing phases, were observed visually in approximately 75% of the column. The remaining upper 25% consisted of a small non-coated sludge fraction that did not consume all available aqueous oxygen. With time, all pyrite grains will be microencapsulated and then oxidation halts completely.

Therefore, the use of fly ash to minimize the environmental impact of pyrite-rich sludge is beneficial. The addi-

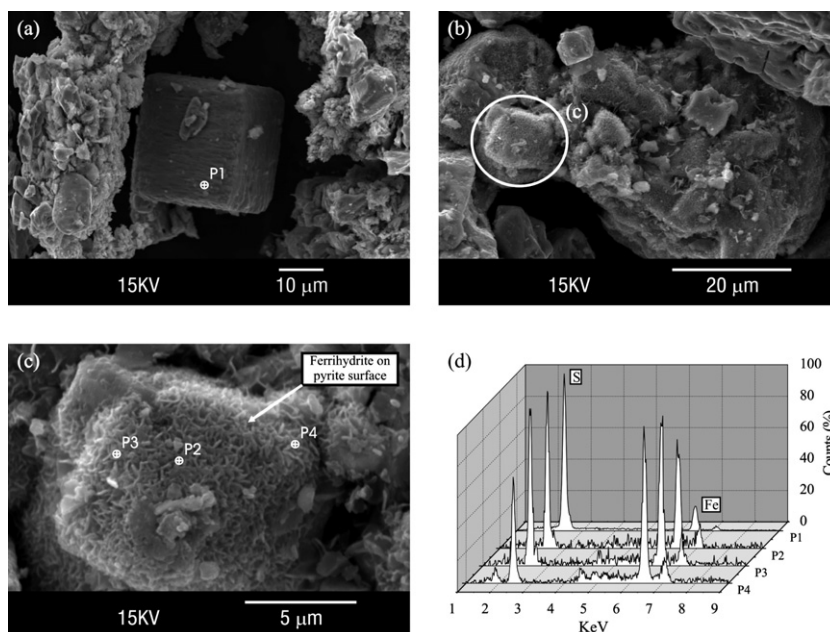


Fig. 10. SEM images of Fe oxyhydroxides coating pyritic grains in saturated column II. (a) Pyrite grains before the experiment; (b) pyrite grains coated with Fe-phases; (c) detail of (b), and (d) EDS patterns (see comments in text).

tion of fly ash to such field residues can potentially contribute to improve the quality of the acid drainage and the development of mechanisms that prevent the AMD production by means of (1) attenuation of pyrite oxidation by Fe-bearing coatings in a short term, as has been discussed in this paper and (2) isolation of the mining waste from weathering by the formation of a rigid crust (hardpan) made up of precipitated minerals in the interface pyrite-rich sludge/fly ash in a medium term, as has been discussed elsewhere (Pérez-López et al., 2005). Moreover, if alkalinity-generating potential of the fly ash was exhausted, the growth of this crust that is facilitated by the cementation of the fly ash would guarantee the isolation of the mining waste.

A full-scale application of the use of fly ash to mitigate AMD was carried out in sulphide mine tailings in Falun, Sweden (Hallberg et al., 2005). The addition of a fly-ash cover upon the tailings favoured the formation of a hardpan that reduces the permeability and oxygen diffusion, resulting in a decrease of the pyrite oxidation rate.

6. CONCLUSIONS

Oxidative dissolution of pyritic tailings from the Iberian Pyrite Belt was studied using non-stirred and stirred flow-through experiments at 22 °C, atmospheric conditions and pH 8.9 (simulating the addition of an alkaline substance). In these conditions, the Fe released during the pyrite oxidation precipitates as ferric oxyhydroxide (ferrihydrite and/or Fe³⁺ amorphous phases). If non-stirred conditions are maintained, the Fe-bearing precipitates form a coating over the pyritic grains that prevents the pyrite dissolution as dissolved oxygen cannot diffuse through the coating to reach the pyrite surface. This Fe-bearing coating formation on pyrite grains that is known as microencapsulation is readily identified by SEM images. Nonetheless if stirring conditions are maintained, Fe-precipitates do not coat the grains and pyrite oxidative dissolution keeps on going.

The main conclusion deduced from these kinetic experiments is that the addition of a substance (e.g., fly ash) that favours the pyrite sludge dissolution in alkaline conditions can induce pyrite microencapsulation in a relatively short term. The prevention of pyrite oxidation contributes to the inhibition of acid mine drainage production, becoming a significant advance in the restoration of numerous sources of AMD pollution. Likewise, the column experiments in the present paper show that the fly-ash is an acidity neutralizing material, whose leaching before sludge dissolution attenuates pyrite oxidation by microencapsulation of pyrite grains.

The potential use of fly ash to attenuate the pyrite oxidation is not limited to its capacity to encapsulate the pyrite grains in a short term, but it can also promote a hardpan in the interface between the fly ash and the pyrite sludge in a medium term that ensures the total neutralization of the mine residues. Therefore, the utilization of fly ash to treat mine residues at the Iberian Pyrite Belt would be beneficial.

ACKNOWLEDGMENTS

This work has been financed through the project REN2003-09590-C03 of the Spanish Ministry of Education and Science

(CICYT). The analytical assistance of Javier Pérez, Rafel Bartrolí, Mercè Cabanes, Josep Elvira from the Institute of Earth Sciences "Jaume Almera" (CSIC) and the technicians at the Central Research Services of the University of Huelva is gratefully acknowledged. We thank the Associate Editor Jacques Schott and two anonymous reviewers for their thorough reviews that significantly improved the quality of the manuscript.

REFERENCES

- Ayala J., Blanco F., García P., Rodríguez P., and Sancho J. (1998) Asturias (Spanish) fly ash as heavy metals removal materials. *Fuel* **77**, 1147–1154.
- Barrante J. R. (1974) *Applied Mathematics for Physical Chemistry*. Prentice-Hall, Englewood, Cliffs, NJ.
- Brake S. S., Jensen R. R., and Mattox J. M. (2003) Effects of coal fly ash amended soils on trace element uptake in plants. *Environ. Geol.* **45**, 680–689.
- Cama J., and Acero P. (2005) Dissolution of minor sulphides present in a pyritic sludge at pH 3 and 25 °C. *Geol. Acta* **3**, 15–26.
- Cama J., Ayora C., Querol X., and Ganor J. (2005) Dissolution kinetics of synthetic zeolite NaP1 and its implication to zeolite treatment of contaminated waters. *Environ. Sci. Technol.* **39**, 4871–4877.
- Dermatas D., and Meng X. (2003) Utilization of fly ash for stabilization/solidification of heavy metal contaminated soils. *Eng. Geol.* **70**, 377–394.
- Domènech C., De Pablo J., and Ayora C. (2002) Oxidative dissolution of pyritic sludge from the Aznalcóllar mine (SW Spain). *Chem. Geol.* **190**, 339–353.
- Evangelou V. P. (1995) *Pyrite Oxidation and Its Control*. CRC Press, Boca Raton, FL.
- Evangelou V. P. (2001) Pyrite microencapsulation technologies: principles and potential field application. *Ecol. Eng.* **17**, 165–178.
- Evangelou V. P., and Huang H. (1993) Infrared spectroscopic evidence of an Iron(II)-carbonate complex on the surface of pyrite. *Spectrochim. Acta* **50A**, 1333–1340.
- Evangelou V. P., Seta A. K., and Holt A. (1998) Potential role of bicarbonate during pyrite oxidation. *Environ. Sci. Technol.* **32**, 2084–2091.
- Hallberg R. O., Granhagen J. R., and Liljemark A. (2005) A fly ash/biosludge dry cover for the mitigation of AMD at the Falun mine. *Chem. Erde* **65**, 43–63.
- Holmes P. R., and Crundwell F. K. (2000) The kinetics of the oxidation of pyrite by ferric ions and dissolved oxygen: an electrochemical study. *Geochim. Cosmochim. Acta* **64**, 263–274.
- Hood Y. A. (1991) The kinetics of pyrite oxidation in marine systems. Ph.D. Thesis, University of Miami, FL.
- Jurjovec J., Ptacek C. J., and Blowes D. W. (2002) Acid neutralization mechanisms and metal release in mine tailings: a laboratory column experiment. *Geochim. Cosmochim. Acta* **66**, 1511–1523.
- Manz O. E. (1997) Worldwide production of coal ash and utilization in concrete and other products. *Fuel* **76**, 691–696.
- McKibben M. A. (1984) Kinetics of aqueous oxidation of pyrite by ferric ion, oxygen and hydrogen peroxide from pH 1–4 and 20–40 °C. Ph.D. Thesis, Pennsylvania State University, USA.
- Moreno N., Querol X., Ayora C., Pereira C. F., and Janssen-Jurkovicova M. (2001) Utilization of zeolites synthesized from coal fly ash for the purification of acid mine waters. *Environ. Sci. Technol.* **35**, 3526–3534.
- Moses C. O., and Herman J. S. (1991) Pyrite oxidation at circumneutral pH. *Geochim. Cosmochim. Acta* **55**, 471–482.

- Mylona E., Xenidis A., and Paspaliaris I. (2000) Inhibition of acid generation from sulphidic wastes by the addition of small amounts of limestone. *Miner. Eng.* **13**, 1161–1175.
- Nicholson R. V., Gillham R. W., and Reardon E. J. (1988) Pyrite oxidation in carbonate-buffered solution: 1. Experimental kinetics. *Geochim. Cosmochim. Acta* **52**, 1077–1085.
- Nicholson R. V., Gillham R. W., and Reardon E. J. (1990) Pyrite oxidation in carbonate-buffered solution: 2. Rate control by oxide coatings. *Geochim. Cosmochim. Acta* **54**, 395–402.
- Oliás M., Nieto J. M., Sarmiento A. M., Cerón J. C., and Cánovas C. R. (2004) Seasonal water quality variations in a river affected by acid mine drainage: the Odiel River (South West Spain). *Sci. Total Environ.* **333**, 267–281.
- Parker G. and Robertson A. (1999) Acid Drainage. A critical review of acid generation from sulfide oxidation: Processes, treatment and control. Australian Minerals & Energy Environment Foundation, Occasional Paper No. 11, 227 pp.
- Parkhurst D. L. (1995) User guide to PHREEQC—a computer program for speciation, reaction-path, advective-transport, and inverse geochemical calculations. US Geological Survey Water Resources Investigation Report 95-4227, Lakewood, Colorado, 143 pp.
- Pérez-López R., Nieto J. M., and Almodóvar G. R. (2005) The use of alkaline residues for the inhibition of acid mine drainage processes in sulphide-rich mining wastes. In *Proceedings of the 9th International Mine Water Association (IMWA) Congress*. Oviedo, Spain, 5–7 September 2005.
- Querol X., Umaña J. C., Alastuey A., Ayora C., Lopez-Soler A., and Plana F. (2001a) Extraction of soluble major and trace elements from fly ash in open and closed leaching systems. *Fuel* **80**, 801–813.
- Querol X., Umaña J. C., Plana F., Alastuey A., Lopez-Soler A., Medinaceli A., Valero A., Domingo M. J., and Garcia-Rojo E. (2001b) Synthesis of zeolites from fly ash at pilot plant scale. Examples of potential applications. *Fuel* **80**, 857–865.
- Singer P. C., and Stumm W. (1970) Acidic mine drainage: the rate-determining step. *Science* **167**, 1121–1123.
- Smith E. E. and Shumate K. S. (1970) Sulfide to sulfate reaction mechanisms. Water pollution control series. 14010 FPS 02/70. USEPA, Washington, DC.
- Vandiviere M. M., and Evangelou V. P. (1998) Comparative testing between conventional and microencapsulation approaches in controlling pyrite oxidation. *J. Geochem. Explor.* **64**, 161–176.
- Verdes G., Gout R., and Castet S. (1992) Thermodynamic properties of the aluminate ion and of bayerite, boehmite, diasporite and gibbsite. *Eur. J. Mineral.* **4**, 767–792.
- Webster J. G., Nordstrom D. K., and Smith K. S. (1994) Transport and natural attenuation of Cu, Zn, As and Fe in the acid mine drainage of Leviathan and Bryant Creeks. In *ACS Symposium series 550 "Environmental Geochemistry of Sulfide Oxidation"* (eds. C.N. Alpers and D.W. Blowes), pp. 244–260.
- Williamson M. A., and Rimstidt J. D. (1994) The kinetics and electrochemical rate-determining step of aqueous pyrite oxidation. *Geochim. Cosmochim. Acta* **58**, 5443–5454.

Associate editor: Jacques Schott